



Phase shifted-lateral shearing digital holographic microscopy imaging for early diagnosis of cysts in soft tissue-mimicking phantom

Tugba Ozge Onur¹ · Gulhan Ustabas Kaya¹ · Ceren Kaya²

Received: 29 August 2020 / Accepted: 17 March 2021 / Published online: 4 April 2021
© The Author(s), under exclusive licence to Springer-Verlag GmbH Germany, part of Springer Nature 2021

Abstract

The diagnosis of cyst structures that can be seen in almost every part of the body can be made using various medical imaging methods recently. Although the used methods and devices provide convenience in diagnosis and treatment, sometimes they can not detect early-stage cyst structures without showing any symptoms. In this study, the cystic structures with different size and formation in phantoms which are soft tissue-mimicking structures created without the need for any living tissue obtained with biopsy process are visualized by the proposed Phase Shifted-Lateral Shearing Digital Holographic Microscopy in three dimensional. The proposed method is verified with experimental results obtained by using various phantom models created at different times and structures. Experimental results illustrate the applicability of the proposed method for imaging of the cyst structures in the created soft tissue-mimicking phantoms even if they are in different structures, formations and stages (especially in early stage). In other respects, it enables to image the biological specimens in small size using simple and low-cost setup.

1 Introduction

Medical imaging takes an important place in the field of medicine in terms of diagnosing and treating the disease. For this reason, the need for innovation and improvements in imaging systems is increasing day by day to examine the internal structure of organs and to ensure early diagnosis and treatment of diseases. In the past decade, there have been various imaging techniques, that have been used by many researchers and scientists to diagnose cyst structures, such as computed tomography (CT), X-ray radiography, elastography, ultrasonography (USG), magnetic resonance imaging (MRI), radionuclide imaging (Scintigraphy), positron emission tomography (PET), single photon emission computed tomography (SPECT) [1–4]. In addition to these techniques, cellular and molecular functions in the body can be shown using light in optical imaging (OI) [5, 6]. Abnormalities and pathological conditions in the tissue are displayed as a result

of the interaction of light with different tissue components via OI [6]. For this context, it is widely used for probing hemodynamics [7], detecting tumors [8], providing functional imaging of the brain [9], scanning the breast cancer [10], the bone health, the teeth, gums and jaws [11]. On the other hand, it has a few disadvantages in the visualization of tissue such as breast. The most important drawback is the low spatial resolution due to the diffusive nature of light propagation in soft tissues such as breast tissue [12]. In this case, sensitivity of the technique in detecting breast lesions decreases in high-density breast tissues which are considered to be more at risk for developing breast cancer [13, 14]. For this reason, to provide early diagnosis and treatment, it is very important to make the technique sensitive for very small lesions or masses.

Conventional optical microscopes are used for cell imaging. However, they can not quantify the cell parameters due to not to measure the spatial phase and refraction index of cells [15]. Therefore, digital holographic microscopy (DHM) is an ideal tool for imaging and characterization of small biological lesions. It enables to directly capture the quantitative phase image of the microscopic objects with high resolution [16, 17]. In addition, focusing of the object in different planes by numerical reconstruction can be achieved without the use of optomechanical adjustment with DHM. Distortions due to deviation in the optical system can be prevented

✉ Tugba Ozge Onur
tozge.ozdinc@beun.edu.tr

¹ Department of Electrical-Electronics Engineering,
Zonguldak Bulent Ecevit University, 67100 Zonguldak,
Turkey

² Department of Biomedical Engineering, Zonguldak Bulent
Ecevit University, 67100 Zonguldak, Turkey

by interferometric matching of the reconstructed phase with and without the object being examined [18, 19].

1.1 Related works and motivation

DHM have been used for the investigation of microscopic objects as biological samples. In the recent past, there have been several attempts. Lam et al. investigated cancer cell morphology by using DHM and machine learning techniques. They distinguished rounded and elongated morphologies of cancer cells with 94% accuracy [20]. El-Schich et al. provided a review study to cancer research using DHM [21]. Anand et al. presented an overview study about DHM applications of 3-dimensional (3D) cell imaging and automated disease identification [15]. The methods of DHM, which are self-referencing geometry and two beam configurations requiring more optical components, are compared in terms of image quality and field of view in their study. They emphasized that lateral shearing DHM provides better quantitative phase images for 3D cell imaging compared to Mach–Zehnder configuration due to less optical element and higher temporal stability and resolution. Vora et al. tested the DHM for imaging and quantifying human red blood cells. In their study, they used lateral shearing- digital holographic interference microscopy to visualize the cells instead of Mach–Zehnder interferometry, which is widely used in DHM. The advantage of this study is being the usable for whole field of view [22]. Moreover, the label-free quantitative phase imaging of biological cells is performed using volume phase holographic grating based on digital holographic interferometer by Rastogi et al. In their work, the coherent noise is reduced by carrying the stray light from the system to the grating. The whole field of view is used by selecting the five platelet cells, where the four cells are at the four corners and one cell is in the center [19].

To image small biological specimens, Singhet et al. proposed to use lateral shearing digital holographic microscopy (LSDHM) [23]. Phase-contrast imaging is achieved and quantitative phase information is also extracted by this method. In LSDHM, two sheared object beams constitute the interference pattern by reflecting the beam from the back and front surfaces of shear glass plate. In the recording camera plane, half of the field of view is used. However, duplicate image problem occurs in this method [23]. On the other hand, Devinder et al. used the subdivided two-beam interference (STBI) system, which is based on LSDHM, to quantitative analyze the numerically focused red blood cells. They also overcome the overlapping problem using STBI system [24]. However, although LSDHM is a common-path system to overcome the stability and more component problems, the self-referencing geometry causes a problem of duplicate image due to self-overlapping of the object beam [23, 25]. One way to solve the duplicate images and object

information overlap is using phase-shifting technique, which is suitable for real-time measurements of nonmoving objects such as very small lesions and masses [26]. In this paper, we propose to adapt the phase shifting technique to LSDHM for imaging the small lesions without overlapping problem.

On the other hand, the samples are obtained from patients clinically by biopsy to image the small lesions or masses in tissues. Ethical permission is also required for the examination of animal and human cells. To eliminate these problems, phantom (artificial tissue) applications have gained importance, recently. It is a great convenience to use phantoms that represent human tissue properties accurately to test and verify new medical imaging systems. In this sense, instead of using real biological tissues, preliminary measurements with phantoms are useful in system testing and accurate calibration [27]. Besides this, in preclinical research, by using tissue-mimicking phantoms as an alternative to *ex vivo* tissues and organs, optimization of therapy protocols is provided without the need for animal or human patients. Until now, ultrasonic imaging devices, microwave holography systems and digital holographic microscopy have been used for imaging tissue-mimicking phantoms [28]. In this context, Karaböce et al. imaged the different objects inside the tissue-mimicking phantom by using ultrasonic imaging device [29]. In addition, Ziemczonok et al. visualized 3D-printed biological cell phantoms using off-axis Mach–Zehnder digital holographic microscope [30]. To the best of authors' knowledge, the tissue-mimicking phantoms imaging with digital holography is very limited in the literature and there has been no work which consider using lateral shearing holographic microscopy to phantom imaging, yet. The analysis in this paper is considered as the first study which applies the phase shifting process to LSDHM for imaging the tissue-mimicking phantoms.

1.2 Contribution

The main contributions of this paper are as follows:

- The phase-shifting process is applied for the first time to LSDHM for imaging the masses in phantom with high spatial resolution and this method is called as PS-LSDHM.
- The mechanical and unwanted vibrations, which occur in the Mach–Zehnder and Michelson interferometers having two beam configurations are reduced without more optical components using proposed PS-LSDHM. Thus, the stability of the system is increased and alignment of setup is adjusted.
- The overlapping problem seen in conventional two beam configurations and common-path LSDHM is overcome with phase shifting process.

- The imaging of created phantom obtained with agar-agar (Agar) is performed using PS-LSDHM in this study to prevent taking clinically by biopsy from patients.
- We present the results by producing different phantoms at different times to validate this study. The thickness and cross-sectional thickness profiles of the cystic structure in the created phantoms are shown.

1.3 Organization

The paper is composed as follows. Fabrication of phantoms is expressed in detail in Sect. 2.1. The basic concept of LSDHM and the application of phase-shifting process with LSDHM are described in Sect. 2.2. Image reconstruction process is explained in detail in Sect. 2.3. The obtained results of the proposed method for phantom is presented in Sect. 3. The imaging of the produced phantoms is enlarged in Sect. 3.1. The resolution of the proposed system has been reviewed in Sect. 3.2. The field of view for self-referencing digital holographic microscope is explained in Sect. 3.3. Finally, in Sect. 4, the conclusion and the future works are summarized.

2 Materials and methods

2.1 Fabrication of phantom

The phantom model used in the experiments is formed with the mixture of agar powder and the distilled water. Agar is a kind of natural gelatin obtained from seaweeds that can be processed as flakes, powders and sheets [31]. Agar will remain solid at higher temperatures unlike gelatin, which melts at body temperature. The use of agar in phantom creation can provide advantages such as endurance, ability to hot-set without refrigeration, reusability, being opaque in color and human tissue-mimicking [32]. Therefore, it is preferred to use agar instead of gelatin in the created phantom.

Agar phantom model was produced using weight percent agar formula (5% agar by weight). The appropriate amount of agar powder (900 g/cm² strength, 38 g for a 5% phantom model) became homogeneous by mixing it in 750 mL of distilled cold water. This mixture was heated with agar stirring periodically for about five minutes and was allowed to begin boiling gently. One teaspoon wheat flour and 5 mL ethanol were added in the mixture at this stage to provide more opacity in 5% agar and remove the bubbles observed in proposed phantom model, respectively.

Phantom model casting was carried out in two stages: the first casting set a base for the cystic mass to be placed upon, and the second casting created a cover to lay over the cysts on the soft tissue. About 93.75 mL hot mix was poured into a reusable glass petri dish [(150 mm (L) × 25 mm (W))] to

set the base, which set at room temperature (approximately 22°C) in about 15–20 mins. In order to prevent solidification, the remaining mixture was kept warm during this period. Cystic masses were created using randomly located seeds of *Nigella sativa*, commonly known as black seed or black cumin. The diameter of the used black seeds varies between a minimum of 2.5 mm and a maximum of 6 mm. These masses were placed on the set agar base before the cover was poured. The remaining approximately 93.75 mL of the hot mixture was poured onto the masses as a cover and left for another 15–20 mins. The cover is set about 1 cm of agar between the surfaces of the cystic mass and the cover. 3 phantom models (Phantom-I, Phantom-II and Phantom-III) including various stages of cystic masses were prepared on 3 different dates. Prepared cystic mass phantom models are given in Fig. 1.

2.2 Experimental setup

In this study, to image the masses in phantom with high spatial resolution and without object information overlapping, phase shifting process is applied to LSDHM. The proposed configuration of Phase-shifting lateral shearing digital holographic microscope is depicted in Fig. 2. The setup derived the self-referencing configuration consists of a light source, spatial filter, lens to expand the beam, microscopic objective for magnification, wave plates to shift the phase, plane ruled reflection grating (PRRG) glass plate and complementary metal-oxide semiconductor (CMOS) camera. A laser beam produced by a He–Ne Laser (632 nm, 12 mW, unpolarized) is spatially filtered by the spatial filter (15 μm pinhole) and collimated by a convex lens (CL) with a focal length of 100 mm. CL is kept 25 cm from the microscopic objective (MO). At first stage the collimated beam directed towards the sample, which is used as masses in phantom in this study, and subsequently magnified by 6X (NA = 0.75) MO. The magnified object wavefront is directed to PRRG glass plate, which is mounted at an angle of 45° (approx.) to the beam. The object wavefront is magnified by falling on a thick (6 mm) PRRG shear glass plate. The distance between MO and PRRG glass plate is taken as 2 cm and the PRRG glass plate is kept 8 cm (approx.) from the CMOS camera. Whole (approx.) field of view (FOV) is used as making equal to the lateral shear distance to get a fringe pattern be equal to that of two-beam interference digital holographic microscopy. The interference pattern (IP) is constituted using two sheared object beams, which are reflected from the back and front surfaces of shear glass plate. IP is captured by a 8 bit CMOS camera with a resolution of 256 × 256 (frame rate 50fps, pixel pitch:14 μm). As a consequence of the self-referencing configuration of this system, the recorded holograms contain with and without object information overlap and duplicate images (See Fig. 2). As this overlap happens, the results

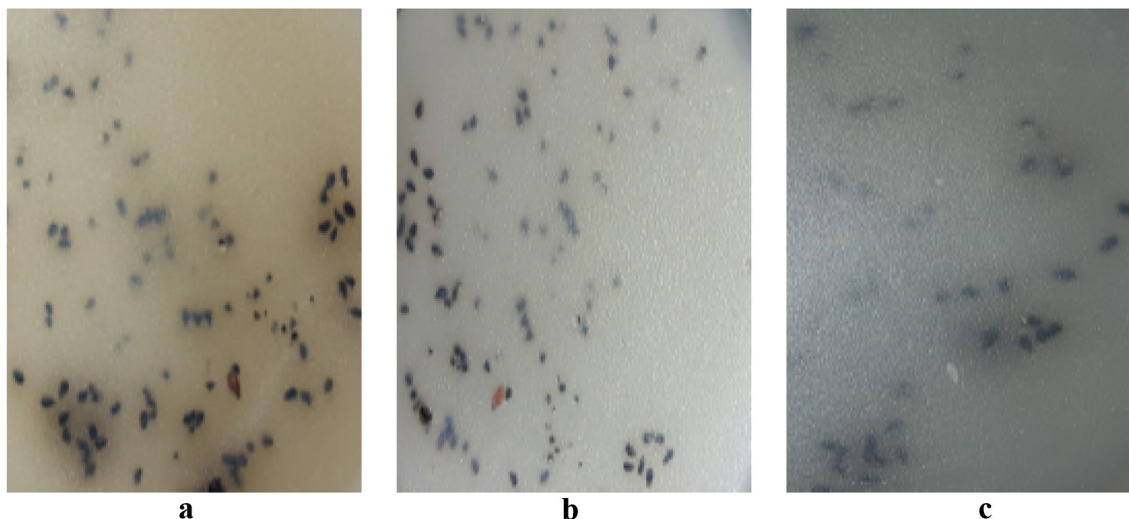


Fig. 1 Cystic mass (5% Agar) phantom models a Phantom-I, b Phantom-II, c Phantom-III

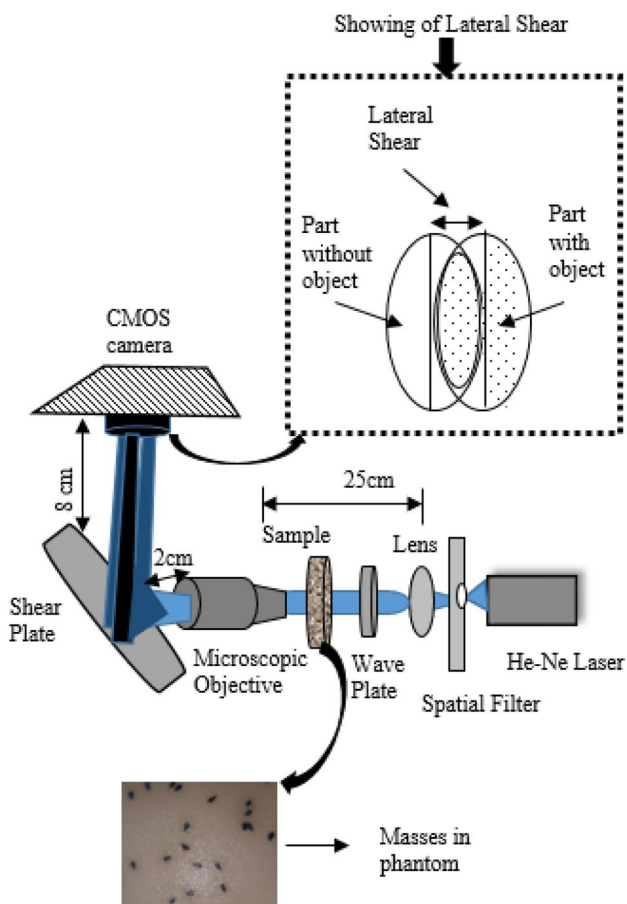


Fig. 2 Schematic of PS-LSDHM with showing lateral shear region and sample

of reconstruction is degraded and the extraction of the phase information obtained from hologram can be difficult.

To overcome the duplicate image and object information overlap problems, phase-shifting technique is applied LSDHM in this study for the first time. Therefore, in the second stage of this part, to record a phase-shifted holograms with LSDHM, the quarter and half-wave plates are used. As shown in Fig. 2, these plates are placed between the sample object (masses in phantom) and the CL. Phase shifting process is performed in four steps. First, the initial phase is accepted to be 0. Then, quarter-wave and half-wave plates are added to the system to shift the phase value $0, \pi/2, \pi, 3\pi/2$, respectively. Hologram recording is performed for each case. The recorded interference patterns include the four different phase-shifted images whose mathematical expressions are given in Eq. (1) [33, 34].

$$\begin{aligned}
 I_0(x, y) &= I_1^2(x, y) + I_2^2(x, y) \\
 &\quad + 2I_1I_2 \cos(\phi(x, y)) \\
 I_{\pi/2}(x, y) &= I_1^2(x, y) + I_2^2(x, y) \\
 &\quad + 2I_1I_2 \cos(\phi(x, y) + (\pi/2)) \\
 I_{\pi(x,y)} &= I_1^2(x, y) + I_2^2(x, y) \\
 &\quad + 2I_1I_2 \cos(\phi(x, y) + (\pi)) \\
 I_{3\pi/2}(x, y) &= I_1^2(x, y) + I_2^2(x, y) \\
 &\quad + 2I_1I_2 \cos(\phi(x, y) + (3\pi/2))
 \end{aligned}
 \tag{1}$$

Here, the coordinates in the hologram plane are defined as (x, y) . In addition, $I_1(x, y)$ represents the altered region and $I_2(x, y)$ refers to the unaltered region of sheared wavefront. They are reflected from the front surface and back surface of the shear plate respectively. Moreover, the intensity of the initial reference fringe pattern is expressed as I_0 with phase retardation angle of $\phi(x, y)$. In conventional systems, the

duplicate image problem is occurred due to more than half of the object beam overlapping with itself. In this paper, this problem is overcome by applying phase shifting to LSDHM.

2.3 Image reconstruction

The quantitative phase information obtained from holograms is reconstructed using phase shifting (PS) reconstruction methods. This method is based on the multiple phase-shifted holograms and enable the suppression of the unwanted zero-order and duplicate images [35, 36]. The principle of phase reconstruction with four-step PS is schematically depicted in Fig. 3.

As seen in Fig. 3, the missing points in the phase information are filled by shifting the phase. Thus, no extra filtering process is required. In this study, the phase and amplitude images are obtained from recorded holograms using PS-LSDHM system. Measured wrapped phase is determined as follows [34]:

$$\phi(x, y) = \alpha \tan 2 \frac{I_{3\pi/2}(x, y) - I_{\pi/2}(x, y)}{I_0(x, y) - I_{\pi}(x, y)} \quad (2)$$

Here, the range of wrapped phase is $[-\pi, \pi]$ and the four-quadrant inverse tangent is defined as $\alpha \tan 2$.

3 Experimental results

3.1 Imaging of the produced phantom

Masses in soft tissues, such as breast, can occur in different sizes and form differently. Therefore, in this study, black seeds which are accepted as cystic structures in the tissue are placed in different sizes and positions in the created phantoms. Holograms recorded using the proposed system are presented in Fig. 4. While the hologram (interference pattern) recorded with the system without using the produced phantom is given in Fig. 4a, the holograms of the regions

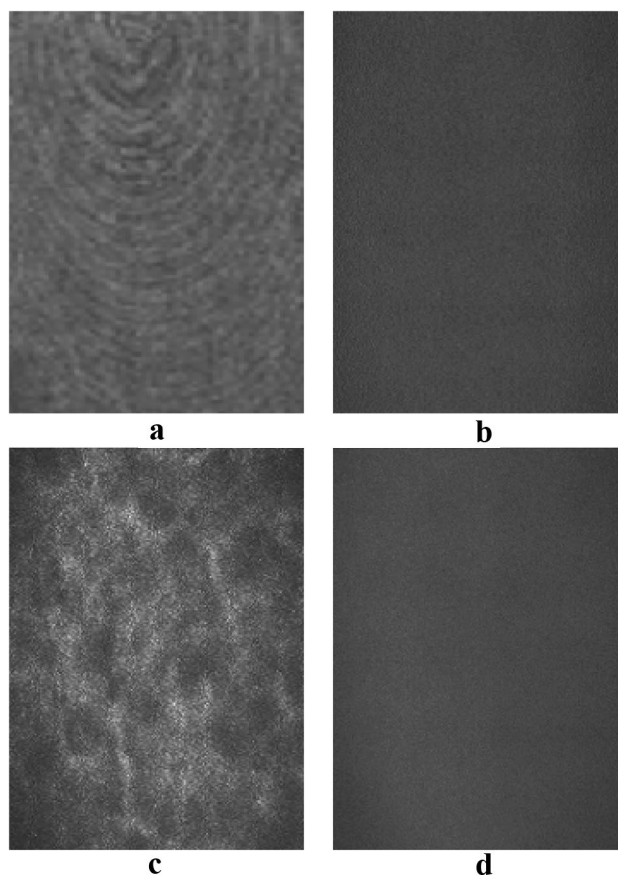


Fig. 4 Recorded reference holograms a hologram without phantom, b hologram of Phantom-I, c hologram of Phantom-II, d hologram of Phantom-III

where the cystic structure is absent in the phantoms presented in Fig. 1 (named as reference hologram) are shown in Fig. 4b–d, respectively.

Later, holograms of cystic structures with different sizes (between the range of 2.5 mm and 6 mm) and positions in 3 different phantoms were produced. The cystic structures to be recorded are shown in Fig. 5 as Phantom-I, Phantom-II

Fig. 3 Principle of phase reconstruction with four-step PS [37]

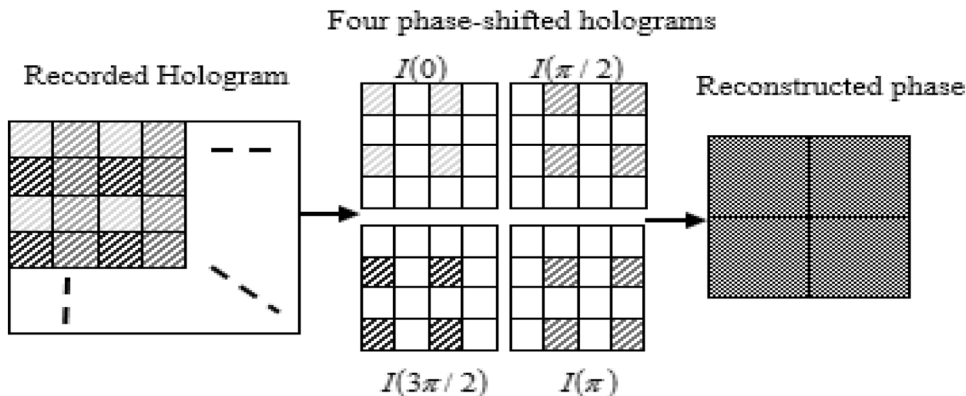
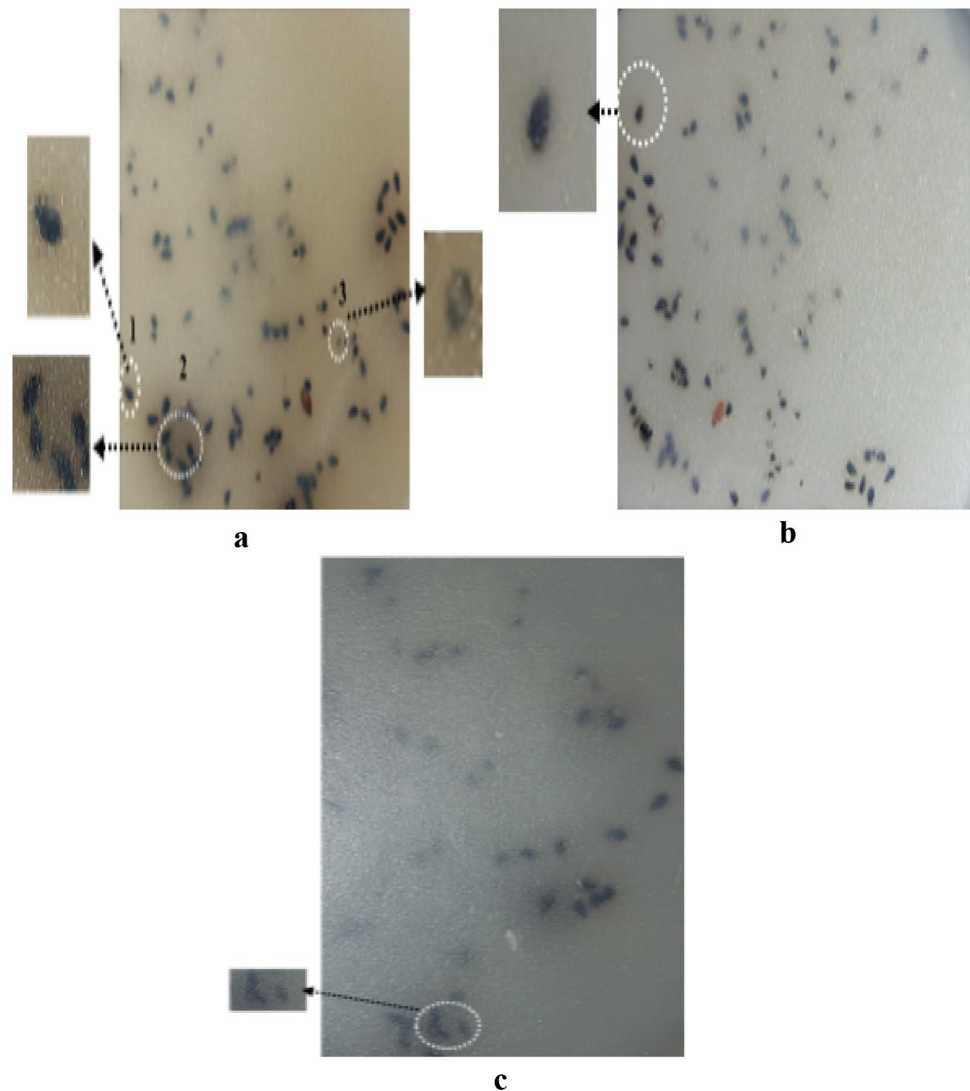


Fig. 5 Marked phantom model
a Phantom-I, **b** Phantom-II, **c**
 Phantom-III



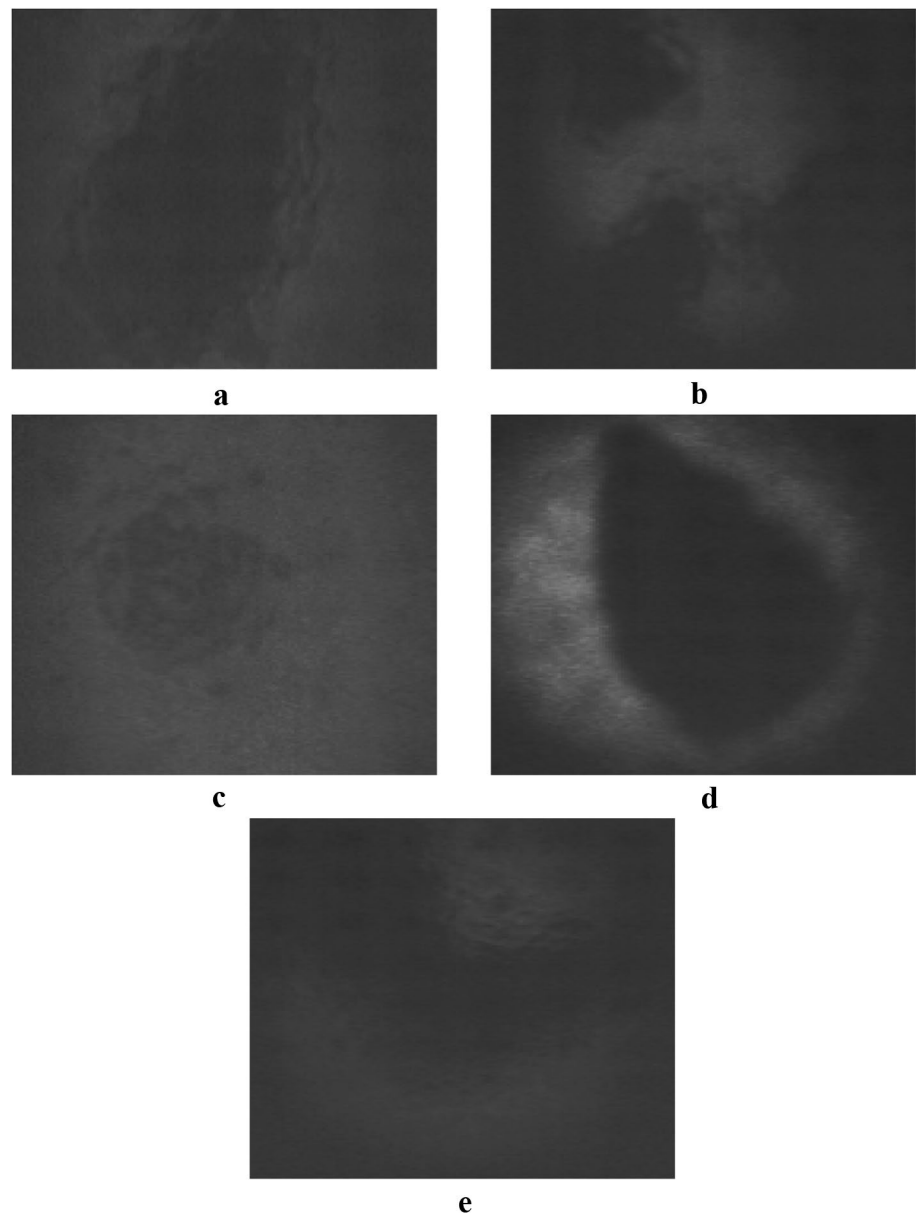
and Phantom-III, respectively. Three different cystic structures (single cystic structure, multiple cystic structure placed side by side and hollow cystic structure, respectively) in Phantom-I are discussed in Fig. 5a. In Fig. 5b, a single cystic structure placed in Phantom-II is examined. The small cystic structure positioned as in the form of "v" in Phantom-III is shown in Fig. 5c.

The whole regions of produced phantoms were not used while recording the process of holograms due to being large. The imaged regions for each produced phantoms are marked in Fig. 5, respectively. If the beam is large enough and the shear is bigger than the object size, the recorded hologram in the field of view contains object information. The diameter of the recorded black seed is also small enough. That's why multiple cystic structure placed side by side can be recorded due to being possible to see more than one black seed in field of view of CMOS camera. The recorded holograms of the cystic structures having different diameters (in

the range of minimum 2.5 mm and maximum 6 mm) used as examples in the system and presented in Fig. 5 are shown in Fig. 6, respectively.

The phase profile was extracted from the recorded holograms (with 256 x 256 pixel value) using Eq. (2). In the stage of calculating phase profile, the phase value was calculated for each pixel, and 3D images were obtained by selecting the maximum points. Thus, the thickness profiles and cross-sectional profiles (for the x and y axes) calculated using the phase distribution were obtained. For marked Phantom-I model (part 1) given in Fig. 6a, reconstructed phase image obtained from recorded holograms, thickness profile and cross-sectional profile are shown in Fig. 7a–c, respectively. In the phase image presented in Fig. 7a, the pixels of (90, 90) points used for the extraction of cross-sectional thickness is shown with the white line on the x and y coordinate axis. This phase image is given as an example and it was not found separately for other examined cystic structures.

Fig. 6 Recorded holograms **a** marked Phantom-I model (part 1), **b** marked Phantom-I model (part 2), **c** marked Phantom-I model (part 3), **d** marked Phantom-II model, **e** marked Phantom-III model



The reconstructed thickness profile and cross-sectional profiles obtained from recorded holograms in Fig. 6b–c are shown in Fig. 8, respectively.

It can be clearly observed that the cystic structure seen in Fig. 7b is narrow and oval in shape, multiple cystic structures are mutually positioned in Fig. 8a, and in Fig. 8b a hollow cystic structure is located in Phantom-I. The cross-sectional thickness profiles presented in Fig. 8 are obtained using the x and y positions selected for the pixel points that are thought to reveal the cystic structure in the thickness profiles of quantitative phase imaging using PS-LSDHM. (50,70), (50,102), (250,155), (150,175) and (140,140) pixel points are chosen for marked Phantom-I model (part 2) and marked Phantom-I model (part 3) given in Fig. 8a and b, respectively.

To deal with cystic structures in different phases and sizes in soft tissue, three different structures are examined in Phantom-I. In this context, it can be observed that in Fig. 8b, there is a hollow cystic structure which represents the stage of formation (early stage); in Fig. 7b there is a single cystic structure depicts to complete its formation and in Fig. 8a describes a cyst structure that grows over time and has more than one cystic structure. With the use of this method, even the cyst structures are at the stage of formation, it enables the detection of cystic structures in the soft tissue at an early stage. In addition, it is thought that it will enable the rapid diagnosis of the disease for both the early stage and the advanced stage and also help the treatment process to start in a short time.

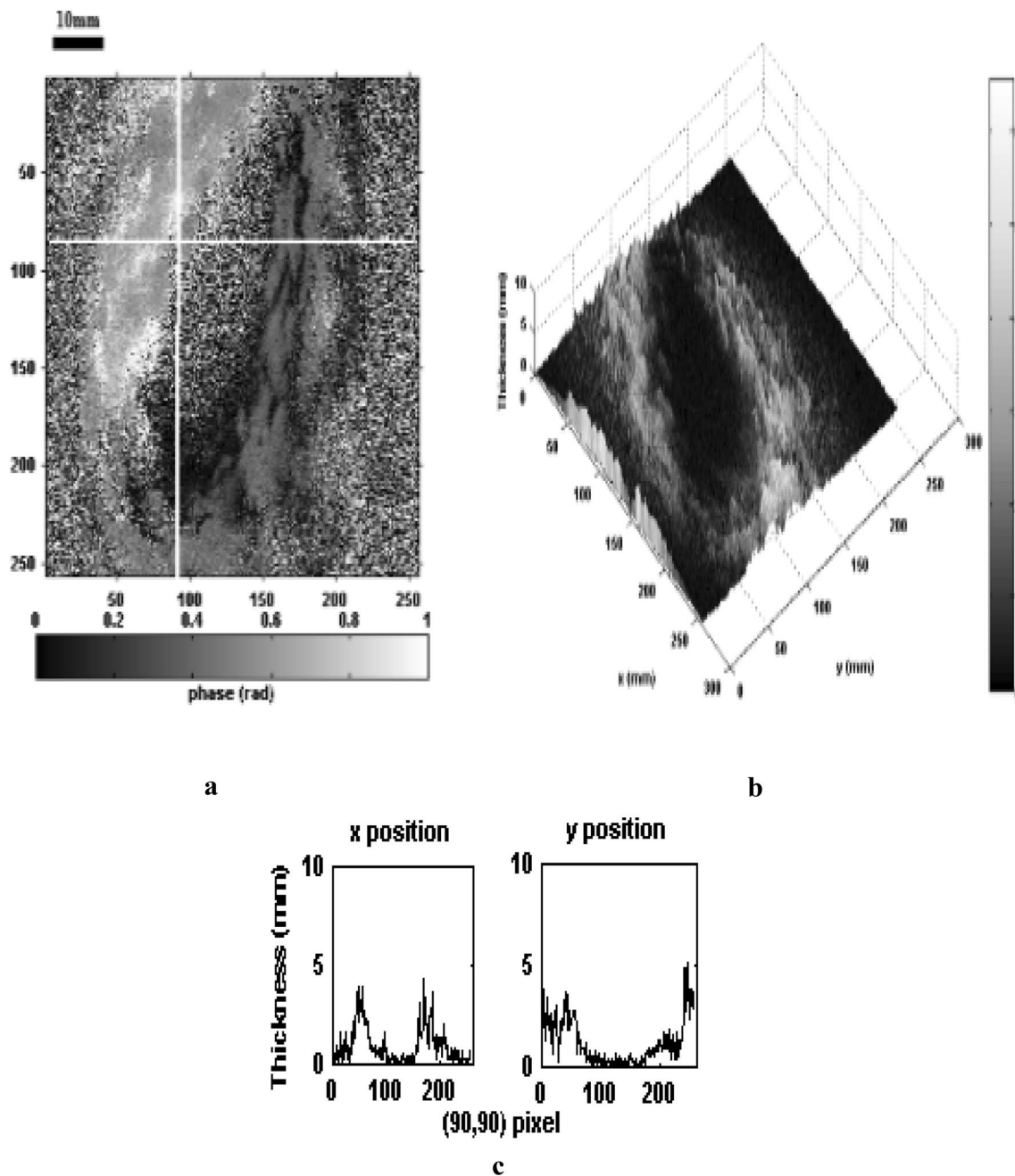


Fig. 7 Quantitative phase imaging using PS-LSDHM for marked Phantom-I model **a** reconstructed phase image, **b** thickness profile, **c** cross-sectional thickness profile obtained from the phase in part 1

The validity of the proposed method is tested by producing different phantoms at different times. For this purpose, the thickness profile and cross-sectional thickness profile of the cystic structure in the Phantom-II model, which is shown by marking in Fig. 5b and given with the hologram in Fig. 6, is presented in Fig. 9. The cross-sectional thickness profile is obtained for (120,187) pixel point.

It is clearly seen that the cystic structure in the Phantom-II model which is shown in detail in Fig. 5b is the same as

the figure obtained for the thickness profile (See Fig. 9) from the recorded hologram of this structure. This cystic structure which is splay shaped, differs from the oval cystic structure given in Fig. 7b.

Finally in this study, the phantom model (Phantom-III model) produced by different positioning of the cystic structures is displayed with the proposed system. The cystic structure is kept in a ‘v’ position. In addition, a small round cystic piece is placed on opposite of this

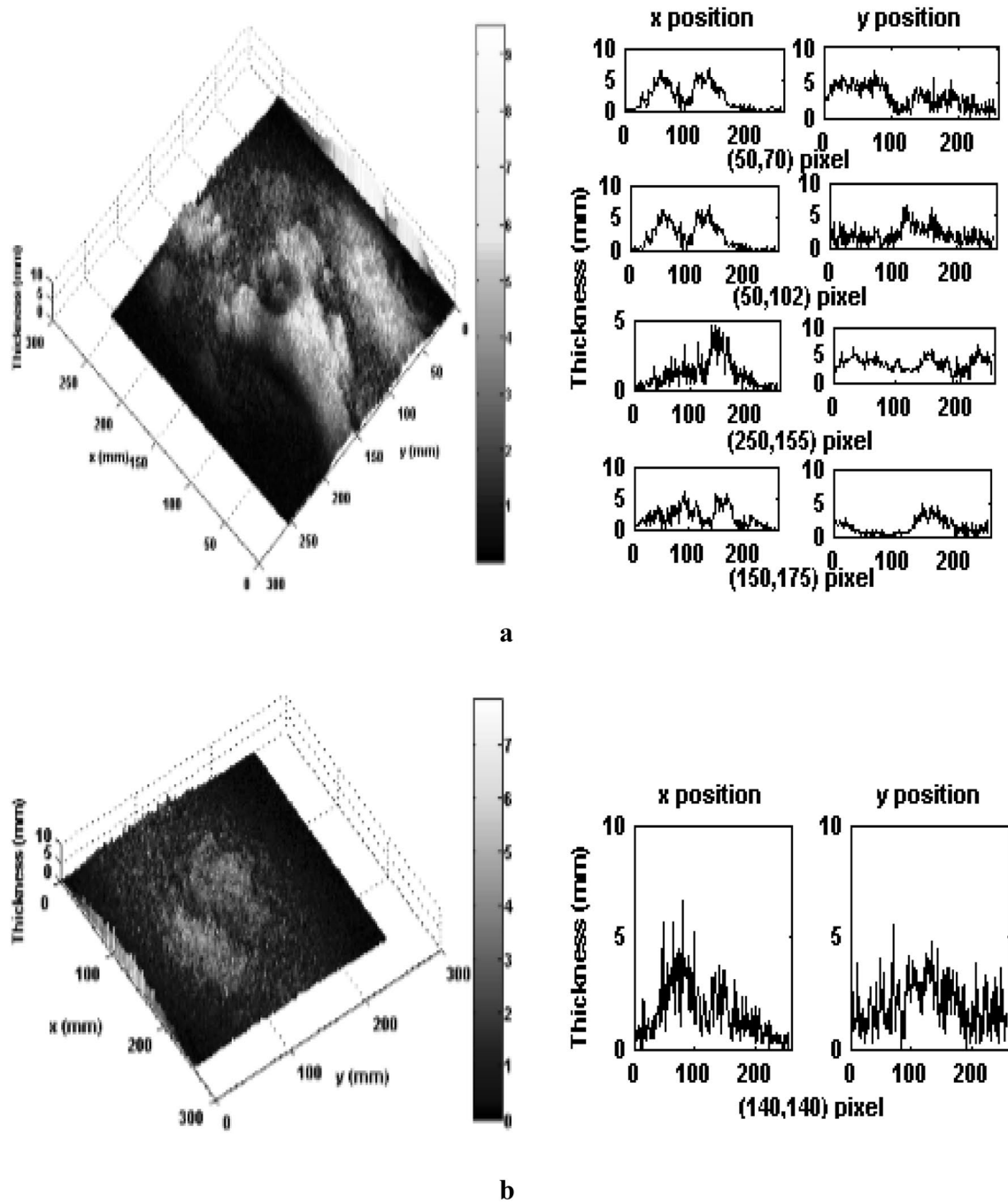


Fig. 8 Quantitative phase imaging using PS-LSDHM **a** thickness profile and cross-sectional thickness profiles obtained from the phase in part 2, **b** thickness profile and cross-sectional thickness profiles obtained from the phase in part 3

structure. The thickness profile and the cross-sectional thickness profiles obtained from holograms recorded for Phantom-III model are shown in Fig. 10.

(127, 260) pixel point of marked Phantom-III is determined in order to obtain the thickness profile and

Fig. 9 Quantitative phase imaging using PS- LSDHM. Marked Phantom-II model; Thickness profile and cross-sectional thickness profiles obtained from the phase-in marked part

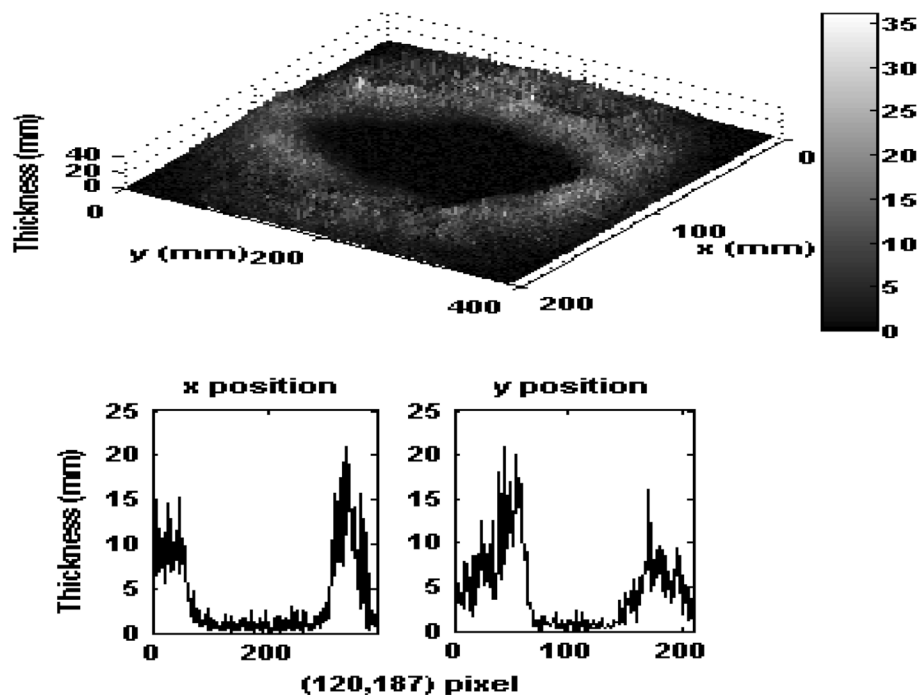
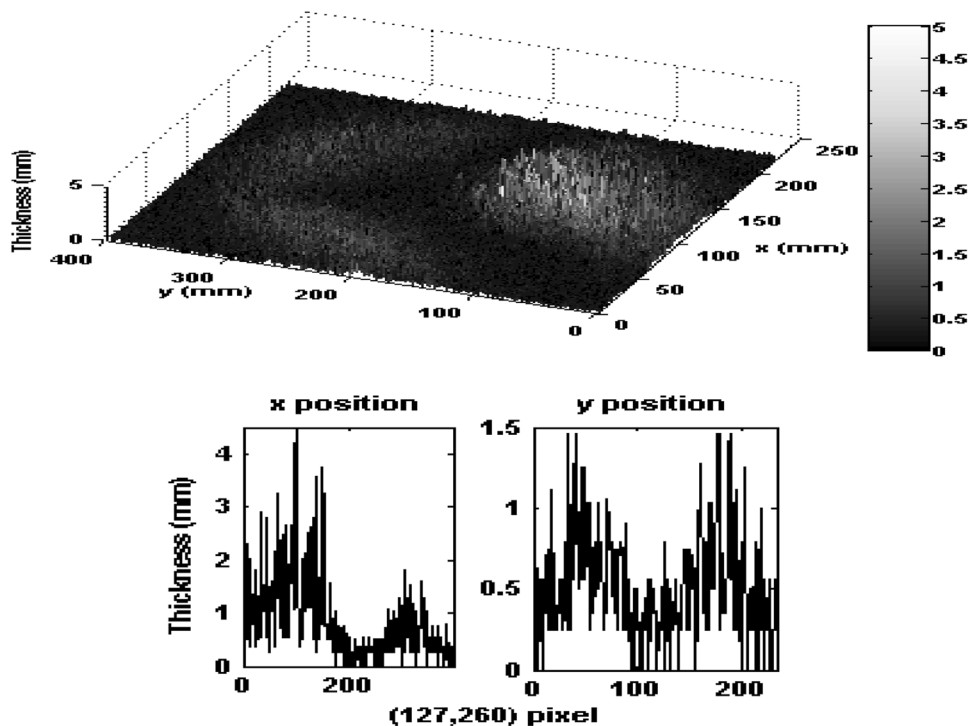


Fig. 10 Quantitative phase imaging using PS- LSDHM. Marked Phantom-III model; Thickness profile and cross-sectional thickness profiles obtained from the phase-in marked part



cross-sectional thickness profiles given in Fig. 10. Thus, the peaks and through points of the cystic structure can be observed clearly.

3.2 Resolution of the proposed system

In this study, to record the holograms, Optronis CamRecord CR600x2 series CMOS camera, which has the highest light sensitivity, is used. This camera records 500 frames per seconds (fps) with a full resolution of 1280×1024 pixels. In the

X and Y pixels, the resolution can be adjusted. If the lower refresh rate of the image is used, the full resolution can be changed [38]. In this study, phantoms are produced using black seeds with sizes ranging between 2.5 mm and 6 mm. In this context, the dimensions of the phantom samples to be recorded as holograms will change in this range. However, since the MO used has 6x magnification, the size of the object to be recorded will be between 15 mm and 36 mm. In this case, to get the best resolution image with this system, the distance between the recording camera used in the system and the MO should be adjusted correctly. To show the resolution of the system, the focal length can be calculated using Eqs. (3) and (4), which are depended on the objects of different sizes and the distance [39].

$$\text{Focal length(mm)} = \frac{A}{1 + \frac{B}{\text{Sensor size(mm)}}} \quad (3)$$

$$\text{Sensor size(mm)} = 0.014\sqrt{C^2 + D^2} \quad (4)$$

Here, A is defined as the distance between the object and the camera lens, and B is the size of the object to be recorded. C and D show the number of horizontal and vertical pixels, respectively. In order to show the relationship between the focal length and maximum camera resolution (1280×1024), the distance between MO and camera is taken as an example at any value. In this context, the distance between MO and camera is taken as an example of 34 mm for black seed phantoms of 2.5 mm (assumed to be 15 mm with 6x MO magnification) and 6 mm (considered to be 36 mm with 6x MO magnification). The focal lengths are obtained using Eq. (3) as 20.5 mm and 13.25 mm, respectively. When the magnified object sizes are used as 15 mm and 36 mm, the lenses with focal lengths of 20.5 mm and 13.25 mm have to be taken, respectively. The distance from lens of CMOS camera to object (here is MO) can be adjusted for reduced sensor resolution using Eq. (5) [39].

$$\text{Distance to object [mm]} = \text{Local length} \times \left(1 + \frac{\text{Object size}}{\text{Sensor size}}\right) \quad (5)$$

In this study to image the created phantom image, X and Y orientation is configured at 256×256 resolution (reduced sensor resolution) with 50fps. Therefore, the MO is kept at distance of 81.2 mm and 107.5 mm from the lens for magnified size of 15 mm and 36 mm phantoms using Eq. (3). Thus, the image with maximum resolution has been obtained.

3.3 Field of view (FOV) for the experimental system

A He–Ne laser module with 632 nm (12 mW, unpolarized) wavelength is used as the light source for a wide field of view LSDHM. In addition, a MO lens (6x magnification and

NA= 0.75) is used to provide the magnification of the object. The spatially filtered laser beam produced by a He–Ne laser is produced and collimated by a CL with a focal length of 100 mm. The CL is kept 25 cm from the MO. At the first stage, the collimated beam directed towards the masses in phantom and magnified by MO lens. The PRRG glass plate is mounted at an angle of 45° (approx.) to the beam and the magnified object wavefront is directed to this plate. The reflected sheared object beams from the back and front surfaces of shear glass plate constitute the IP. If the distance from CMOS lens to object is defined with high resolution, the lateral shear distance can be adjusted.

In conventional studies related with FOV, the difference between the path lengths among the wavefronts can be obtained using Snell's law as explained in Ref. [22] or minimum FOV value can be calculated as given in Ref. [40]. In addition, conventionally, if the lateral shear distance is not taken equal to the minimum half of the FOV, duplicate images can be included in the recorded hologram and overlapped information can be obtained due to the interference between two sheared object beams. In this study, in order to overcome the duplicate image problem, phase-shifting technique is applied to LSDHM as defined in Eq. (1) and in the proposed setup quarter and half-wave plates are used. As for that the FOV of the system, it is not calculated in details in this study. However, under the consideration of the system resolution, which is mentioned in Sect. 3.2 above, the whole (approx.) field of view is used by making equal to the lateral shear distance. We also base on the distance from lens of CMOS camera to object to calculate the lateral shear distance.

4 Conclusion

Soft tissue cysts, like most of the cysts formed in the body, do not show any symptoms in the early stages and the diagnosis can be made in the later stages. These masses in soft tissue can occur in different sizes and ways. They may be in millimeter size or may grow over time and create some threats in the body. Cysts do not cause any symptoms unless they are very large in size. Although there have been various techniques in order to image soft tissues such as breast, they usually fail when cyst lesions are very small and in early stages. In this study, the performance of the proposed PS-LSDHM method with cystic structure lesions of different sizes and structures created with black seed placed in soft tissue mimicking phantom is investigated. The main advantage of the developed PS-LSDHM method is that its whole (approx.) field of view is usable without any redundant object information. In comparison with the two-beam Mach–Zehnder-based microscope, the proposed technique is more temporally stable, providing temporal resolution

and overcoming duplicate image problem by applying phase shifting to LSDHM and using the whole (approx.) FOV. Therefore, since this method avoids overlapping, it works well for the produced cyst structures. For all applications performed in this study, it can be seen that even if the diameter, location, and structure of the cyst structure changes, the proposed imaging method fully reveals the cyst structure in the region being displayed. So, it enables to detect the formed cyst structure in the early stages especially without symptoms. Thus, even if the cyst structures are benign, it will enable early diagnosis and treatment without growing or damaging the surrounding tissues. In addition, the use of phantoms created for the test of the proposed imaging method enable the formation of a soft tissue-mimicking structure without the need for biopsy or any ethical consents to obtain any living tissue. It also provides advantages such as easy production, reusability and low cost. Therefore, phantom models given in this study can be a cost-effective alternative, especially in imaging and testing applications. In the light of all the findings, we hope our study may give new insights for the detection of the cystic structures in the early stages among imaging methods present in the literature. As a future work, we plan to create another tissue-mimicking phantoms and compare its performance with the current study. Also, we plan to develop the proposed imaging method with the use of a different setup.

References

1. H. Kasban, M.A.M. El-Bendary, D.H. Salama, A comparative study of medical imaging techniques. *Int. J. Inf. Sci. Intell. Syst. (IJISR)* **4**(2), 37–58 (2015)
2. J.Z. Cheng et al., Computer-aided diagnosis with deep learning architecture: applications to breast lesions in US images and pulmonary nodules in CT scans. *Sci. Rep.* **6**(1), 1–13 (2016)
3. Y. Lee, Improved total-variation noise-reduction technique with gradient method using iteration counter and its application in medical diagnostic chest and abdominal X-ray imaging. *Optik* **170**(1), 475–483 (2018)
4. E.K. Wang et al., A deep learning based medical image segmentation technique in Internet-of-Medical-Things domain. *Futur. Gener. Comp. Syst.* **108**, 135–144 (2020)
5. J.P. Angelo et al., Review of structured light in diffuse optical imaging. *J. Biomed. Opt.* **24**(7), 071602 (2019)
6. X. Dang et al., Deep-tissue optical imaging of near cellular-sized features. *Sci. Rep.* **9**(1), 1–12 (2019)
7. P. Farzam et al., Shedding light on the neonatal brain: probing cerebral hemodynamics by diffuse optical spectroscopic methods. *Sci. Rep.* **7**(1), 1–10 (2017)
8. N. Honda et al., Determination of optical properties of human brain tumor tissues from 350 to 1000 nm to investigate the cause of false negatives in fluorescence-guided resection with 5-aminolevulinic acid. *J. Biomed. Opt.* **23**(7), 075006 (2018)
9. F. Vasefi, N. MacKinnon, D.L. Farkas, B. Kateb, Review of the potential of optical technologies for cancer diagnosis in neurosurgery: a step toward intraoperative neurophotonics. *Neurophotonics* **4**(1), 011010 (2017)
10. B.M. Haas et al., Comparison of tomosynthesis plus digital mammography and digital mammography alone for breast cancer screening. *Radiology* **269**(3), 694–700 (2013)
11. I.M. Berke et al., Seeing through musculoskeletal tissues: improving in situ imaging of bone and the lacunar canalicular system through optical clearing. *PLoS One* **11**(3), 1–29 (2016)
12. J. Garrett, E. Fear, A new breast phantom with a durable skin layer for microwave breast imaging. *IEEE Trans. Antennas Propag.* **63**(4), 1693–1700 (2015)
13. T.D. Vreugdenburg, C.D. Willis, L. Mundy, J.E. Hiller, A systematic review of elastography, electrical impedance scanning, and digital infrared thermography for breast cancer screening and diagnosis. *Breast Cancer Res. Treat.* **137**(3), 665–676 (2013)
14. Y. Xiao, Q. Zhou, Z. Chen, Automated breast volume scanning versus conventional ultrasound in breast cancer screening. *Acad. Radiol.* **22**(3), 387–399 (2015)
15. A. Anand, I. Moon, B. Javidi, Automated disease identification with 3-D optical imaging: a medical diagnostic tool. *Proc. IEEE* **105**(5), 924–946 (2017)
16. A. Anand et al., Compact, common path quantitative phase microscopic techniques for imaging cell dynamics. *Pramana* **82**(1), 71–78 (2014)
17. Y. Park, C. Depeursinge, G. Popescu, Quantitative phase imaging in biomedicine. *Nat. Photon.* **12**(10), 578–589 (2018)
18. V. Kumar, G.S. Khan., C. Shakher, Phase contrast imaging of red blood cells using digital holographic interferometric microscope. *Proc. SPIE* **10453** Third International Conference on Applications of Optics and Photonics, (2017) pp. 104532T
19. V. Rastogi et al., Design and development of volume phase holographic grating based digital holographic interferometer for label free quantitative cell imaging. *Appl. Opt.* **59**(12), 3773–3783 (2020)
20. V.K. Lam et al., Quantitative assessment of cancer cell morphology and motility using telecentric digital holographic microscopy and machine learning. *Cytom. Part A* **93**(3), 334–345 (2018)
21. Z. El-Schich, A.L. Mölder, A.G. Wingren, Quantitative phase imaging for label-free analysis of cancer cells-focus on digital holographic microscopy. *Appl. Sci.* **8**(7), 1027 (2018)
22. P. Vora et al., Wide field of view common-path lateral-shearing digital holographic interference microscope. *J. Biomed. Opt.* **22**(12), 126001(1–11) (2017)
23. A.S. Singh, A. Anand, R.A. Leitgeb, B. Javidi, Lateral shearing digital holographic imaging of small biological specimens. *Opt. Express* **20**(21), 23617–23622 (2012)
24. S. Devinder, A. Lal, T.R. Dastidar, S.K. Dubey, Quantitative analysis of numerically focused red blood cells using subdivided two-beam interference (STBI) based lateral-shearing digital holographic microscope, [Online]. Available: arXiv preprint [arXiv:1909.03454](https://arxiv.org/abs/1909.03454), (2019)
25. J. Di et al., Dual-wavelength common-path digital holographic microscopy for quantitative phase imaging based on lateral shearing interferometry. *Appl. Opt.* **55**(26), 7287–7293 (2016)
26. P. Marquet, C. Depeursinge, P.J. Magistretti, Review of quantitative phase-digital holographic microscopy: promising novel imaging technique to resolve neuronal network activity and identify cellular biomarkers of psychiatric disorders. *Neurophotonics* **1**(2), 020901 (2014)
27. Y. Cao, G.Y. Li, X. Zhang, Y.L. Liu, Tissue-mimicking materials for elastography phantoms: a review. *Extreme Mech. Lett.* **17**(1), 62–70 (2017)
28. V. Kumari, G. Sheoran, T. Kanumuri, SAR analysis of directive antenna on anatomically real breast phantoms for microwave holography. *Microw. Opt. Techn. Lett.* **62**(1), 466–473 (2020)
29. B. Karaböce, E. Çetin, M. Özdingiş, H.O. Durmuş, Image measurement verification studies of different objects in tissue-mimicking fantom, in *Proc. TIPTEKNO*, (2017) pp. 1-4

30. M. Ziemczonok, A. Kuś, P. Wasylczyk, M. Kujawińska, 3D-printed biological cell phantom for testing 3D quantitative phase imaging systems. *Sci. Rep.* **9**(1), 1–9 (2019)
31. W.K. Lee et al., Biosynthesis of agar in red seaweeds: a review. *Carbohydr. Polym.* **164** (2017)
32. M. Earle, G. De Portu, E. DeVos, Agar ultrasound phantoms for low-cost training without refrigeration. *Afr. J. Emerg. Med.* **6**(1), 18–23 (2016)
33. T. Tahara et al., High-speed three-dimensional microscope for based dynamically moving biological objects based on parallel phase-shift digital holographic microscopy. *IEEE J. Sel. Top. Quantum Electron.* **18**(4), 1387–1393 (2012)
34. T. Kreis, *Handbook of Holographic Interferometry: Optical and Digital Methods*, 2nd edn. (Wiley-VCH, Weinheim, 2005).
35. T. Fukuda et al., Three-dimensional motion-picture imaging of dynamic object by parallel-phase-shifting digital holographic microscopy using an inverted magnification optical system. *Opt. Rev.* **24**(2), 206–211 (2017)
36. T. Fukuda et al., Three-dimensional imaging of distribution of refractive index by parallel phase-shifting digital holography using Abel inversion. *Opt. Express* **25**(15), 18066–18071 (2017)
37. K. Ishikawa et al., High-speed imaging of sound using parallel phase-shifting interferometry. *Opt. Express* **24**(12), 12922–12932 (2016)
38. CR600x2 Product information, <http://optronis.com/en/products/cr600x2-mc/>
39. CR600x2 Camera Users' Manual, <http://optronis.com/nwp-content/uploads/2017/02/Camera-manual-english-1830-SU-02-N.pdf>
40. E. Sánchez-Ortiga et al., Off-axis digital holographic microscopy: practical design parameters for operating at diffraction limit. *Appl. Opt.* **53**(10), 2058–2066 (2014)

Publisher's Note Springer Nature remains neutral with regard to jurisdictional claims in published maps and institutional affiliations.